PHOTONICS Research

Topological protection of partially coherent light

Konrad Tschernig,[1,2,5] Gabriel Martinez-Niconoff,[3] Kurt Busch,[1,2] Miguel A. Bandres,[4,6] and Armando Perez-Leija[1,4,*]

[1]Max-Born-Institut, 12489 Berlin, Germany
[2]Humboldt-Universität zu Berlin, Institut für Physik, AG Theoretische Optik & Photonik, 12489 Berlin, Germany
[3]Coordinación de Óptica, Instituto Nacional de Astrofísica, Óptica, y Electrónica, 72840 Tonantzintla, Puebla, Mexico
[4]CREOL, The College of Optics and Photonics, University of Central Florida, Orlando, Florida 32816, USA
[5]e-mail: konrad.tschernig@mbi-berlin.de
[6]e-mail: bandres@creol.ucf.edu
*Corresponding author: aleija@creol.ucf.edu

Received 13 January 2022; revised 4 March 2022; accepted 4 March 2022; posted 7 March 2022 (Doc. ID 453603); published 14 April 2022

Topological physics exploits concepts from geometry and topology to implement systems capable of guiding waves in an unprecedented fashion. These ideas have led to the development of photonic topological insulators, which are optical systems whose eigenspectral topology allows the creation of light states that propagate along the edge of the system without any coupling into the bulk or backscattering even in the presence of disorder. Indeed, topological protection is a fully coherent effect, and it is not clear to what extent topological effects endure when the wavefronts become partially coherent. Here, we study the interplay of topological protection and the degree of spatial coherence of classical light propagating in disordered photonic topological insulators. Our results reveal the existence of a well-defined spectral window in which partially coherent light is topologically protected. This opens up the design space to a wider selection of light sources, possibly yielding smaller, cheaper, and more robust devices based on the topological transport of light.

https://doi.org/10.1364/PRJ.453603

1. INTRODUCTION

Topological insulators are materials in which the topology of the underlying energy spectra fully disallows the energy transport into the bulk and keeps it circulating along the edges [1]. Topological insulators were discovered in the context of single-particle condensed matter physics [2], and as such they have inspired the quest for topological phases in classical-wave systems [3], including microwave [1], photonic [4–9], and acoustic systems [10,11]. At the forefront, photonics has become one of the most prolific and fertile grounds to study and observe topological effects using so-called photonic topological insulators [12]. Indeed, optics has recently witnessed the experimental demonstration of Floquet topological insulators [4], the quantum Hall effect [6], topological lasers [13,14], and aperiodic topological systems in which the topology is induced by disorder (e.g., topological quasicrystals [15], topological Anderson insulators [16], topological insulators in fractal lattices [17]). Notably, in these latter systems the aperiodicity and disorder have a dramatic impact on the physical properties, not only modifying the topology of the spectra but also creating a topological order in otherwise topologically trivial systems. Concurrently, in the context of quantum optics there have emerged very appealing theoretical and experimental studies of topological protection of entangled states of several photons [18–23].

Thus far, topological protection has been mainly studied for fully coherent waves, and it is not clear to what extent topological effects endure when the excitation fields become incoherent. More generally, we raise the question as to whether an ensemble of weakly correlated light fields—such as those representing partially coherent wavefronts—can be protected in photonic topological insulators. Addressing this question is of considerable importance, as all optical fields undergo random fluctuations that may be small, as in many lasers, or large, as in light generated by thermal sources.

Here, we theoretically investigate the topological protection of partially coherent light propagating through disordered photonic topological insulators and uncover the aspects of light correlations that survive. This endeavor is appealing beyond the previously reported advantages of photonic topological insulators because it addresses the interplay between disorder in topological systems and disorder in the excitation field, and it opens exciting possibilities at the interface of topological physics and partial coherence, such as topologically protected transport in systems with random illumination.

2. PARTIALLY COHERENT LIGHT IN DISORDERED PHOTONIC TOPOLOGICAL INSULATORS

To analyze the topological protection of partially coherent light, we consider a continuous set of light fields that range

from the fully coherent to the fully incoherent limit. In practice, such partially coherent waves are generated in common light sources such as diode-pumped solid-state lasers, laser diodes, light-emitting diodes, superluminescent light-emitting diodes, and micro light-emitting diodes. In this list we have ordered the light sources from the most coherent (solid-state lasers) to the most incoherent ones (light-emitting diodes) [24].

For concreteness, we perform our analysis using the archetypal Haldane model, which exhibits all the essential features of topological insulators such as time reversal-broken symmetry [2]. In optics, the Haldane model is implemented in a finite honeycomb lattice of helical waveguides [4], where each site is coupled to its nearest neighbors by a real hopping parameter κ_1 and to its next-nearest neighbors by a complex parameter $\kappa_2 \exp(i\varphi)$, where φ is the Haldane flux [2]. The Haldane model exhibits two phases: the trivial phase when φ is equal to 0 or π, and the topological phase when $\varphi \in (0, \pi)$. In the topological phase, the system supports edge states with propagation eigenvalues lying in the topological gap, which is proportional to $\kappa_2 \sin\varphi$, reaching its maximum at $\varphi = \pi/2$. Hence, the coupling matrix elements of a disordered Haldane lattice are given by $H_{m,n} = \delta_{m,n}\Delta_n + \kappa_1 \sum_{\langle j,k\rangle}(\delta_{n,j}\delta_{k,m} + \delta_{m,j}\delta_{n,k}) + i\kappa_2 \sum_{\langle\langle j,k\rangle\rangle}(\delta_{n,j}\delta_{k,m} - \delta_{m,j}\delta_{n,k})$, where we have chosen $\varphi = \pi/2$, and the symbols $\langle\rangle$ and $\langle\langle\rangle\rangle$ indicate summation over the nearest and next-nearest-neighbor waveguides, respectively. The term $\delta_{m,n}\Delta_n$ represents the disordered on-site refractive indices, which are generated using a truncated (to full width at half-maximum) normal distribution of unit width, zero mean, and scaled by the disorder strength parameter Δ; see Fig. 1(a). Note, the Kronecker delta ($\delta_{n,m} = 1$ if $n = m$ and $\delta_{n,m} = 0$ otherwise) guarantees that only the diagonal terms of the Hamiltonian are subject to disorder. Furthermore, we use the particular (normalized) nearest-neighbor couplings $\kappa_1 = 1$ and next-nearest-neighbor couplings $\kappa_2 = 1/5$, such that the system exhibits edge modes within the bulk gap $\Delta_b \approx 2$ [Fig. 1(a)]. Throughout this work we normalized the units in terms of κ_1. It is important to point out that the Hamiltonian matrix given above is the effective Hamiltonian after one Floquet period $Z = 2\pi/\Omega$ of the helically modulated waveguide array. The effective next-nearest-neighbor coupling coefficient κ_2 is therefore given in terms of the modulation frequency Ω, the helix radius R, the nearest-neighbor distance (lattice constant) a, and the wavelength λ of the incident light, $\kappa_2 = \sqrt{3}\frac{\kappa_1^2}{\Omega} J_1^2(\frac{2\pi}{\lambda} aR\Omega)$ [25], which is valid only for small arguments of the Bessel function J_1. This relation grants enough degrees of freedom to fulfill our choice $\kappa_2 = \kappa_1/5$, while also maintaining the adiabatic condition, which ensures minimal bending losses.

For scalar wavefronts, a partially coherent wave is described by the mutual intensity function $\hat{\rho}(\boldsymbol{x_1}, \boldsymbol{x_2}; z) = \langle E(\boldsymbol{x_1}, z) E^*(\boldsymbol{x_2}, z)\rangle$ [26], where $E(\boldsymbol{x}, z)$ represents the scalar field along the transverse vector $\boldsymbol{x}$, and the angle bracket denotes time average or ensemble average, which is characterized by the coherence properties of the wavefront at the plane z. For linear waveguide lattices, the evolution of $\hat{\rho}(\boldsymbol{x_1}, \boldsymbol{x_2}; z)$ is governed by Liouville's equation

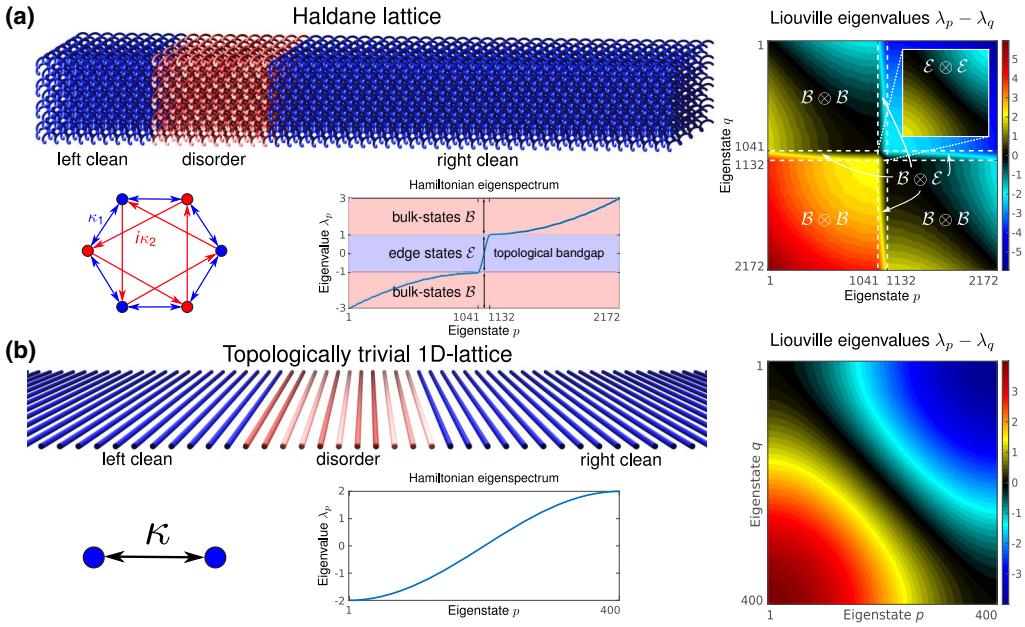

Fig. 1. Haldane lattice. (a) Photonic topological insulator implemented using a honeycomb lattice of helical waveguides with coupling coefficients as described in the hexagonal cell. For fully coherent light, the eigenspectrum exhibits two regions of bulk states and a gap crossed by the edge states $\mathcal{E}$. For our analysis, we consider a lattice consisting of 11 hexagonal cells in the vertical direction and 90 in the horizontal, $\kappa_1 = 1$, and $\kappa_2 = 1/5$. (b) Trivial 1D lattice with couplings κ. In the absence of disorder, the discrete eigenspectrum exhibits a sinusoidal shape, and the corresponding Liouville eigenvalues are degenerated. In both cases, the Liouville eigenspectrum is shown in the right column for the disorder-free systems. The disordered regions (red waveguides) encompass 20 waveguides in the horizontal direction, the initial states are launched in the left clean regions, and they propagate to the right.

$$i\frac{d\hat{\rho}}{dz} = \mathcal{L}\hat{\rho}, \tag{1}$$

where $\mathcal{L} = (\boldsymbol{H} \otimes \boldsymbol{I} - \boldsymbol{I} \otimes \boldsymbol{H})$. In addition, $\boldsymbol{H}$ is the lattice Hamiltonian (coupling matrix), $\boldsymbol{I}$ is the identity matrix of the same dimensions, and $\hat{\rho}$ is expressed as a vector. The solution to Eq. (1), written in matrix form, is given as $\hat{\rho}(\boldsymbol{x_1}, \boldsymbol{x_2}; z) = U(z)\hat{\rho}(\boldsymbol{x_1}, \boldsymbol{x_2}; 0)U^{\dagger}(z)$, where $U(z) = \exp(-i\boldsymbol{H}z)$ is the evolution operator.

Due to the anti-symmetric nature of $\mathcal{L}$, the eigenspectrum in Liouville space is given by all combinations $\Lambda_{m,n} = \lambda_m - \lambda_n$, where λ_n are the eigenvalues of the Hamiltonian. Consequently, in Liouville space the characteristic bandgap of topological insulators does not exist. Instead, the spectrum exhibits massive degeneracies of edge-edge, edge-bulk, and bulk-bulk coherences, as indicated by the black diagonal region in the right panel of Fig. 1(a).

In general, the mutual intensity $\hat{\rho}(\boldsymbol{x_1}, \boldsymbol{x_2}; z)$ can be expressed as a superposition of coherent modes $\hat{\rho}(\boldsymbol{x_1}, \boldsymbol{x_2}; z) = \sum_k \lambda_k \varphi_k^*(\boldsymbol{x_1})\varphi_k(\boldsymbol{x_2})$, where $\varphi_k(\boldsymbol{x})$ are appropriate eigenfunctions and λ_k are the corresponding eigenvalues [26]. In this framework, a partially coherent field can be thought of as a superposition of spatially coherent but mutually uncorrelated modes φ_k whose powers are λ_k. In consequence, for conservative systems, the eigenvalues λ_k fulfill the condition $\sum_n \lambda_n = 1$. The coherent mode representation allows us to define the square of the overall degree of coherence as $\mu^2 = \sum_n \lambda_n^2 / (\sum_n \lambda_n)^2 = \sum_n \lambda_n^2$ [27], whose inverse is referred to as the Schmidt number $S_N = 1/\mu^2$ [28]. This means that a fully coherent beam ρ_c comprises a single spatial mode, whereas maximally incoherent fields ρ_i are characterized by a uniformly weighted superposition of modes, $\rho_i \propto \boldsymbol{I}$ [26], where $\boldsymbol{I}$ is the identity matrix.

To construct the initial partially coherent fields, we combine the coherent and incoherent extremes

$$\hat{\rho}_\alpha = \alpha\hat{\rho}_c + (1 - \alpha)\hat{\rho}_i, \tag{2}$$

where the real parameter α controls the degree of spatial coherence ($0 \le \alpha \le 1$), with $\alpha = 1$ ($\alpha = 0$) corresponding to a fully coherent (incoherent) field. To generate $\hat{\rho}_c$, we use a discrete Gaussian function $\boldsymbol{E}$ with elements $E_m = A\exp(im\varphi) \cdot \exp(-(m - l)^2/2\sigma^2)$, such that $\hat{\rho}_c = \boldsymbol{E} \otimes \boldsymbol{E}^{\dagger}$, while $\hat{\rho}_i$ is the state obtained from $\hat{\rho}_c$ by deleting all off-diagonal elements to get $[\hat{\rho}_i]_{m,n} = |E_m|^2\delta_{m,n}$; see Fig. 2(a). Here, A is a normalization constant, φ is an appropriate phase that imprints the proper momentum onto the wave packets, l is the spatial center, and σ defines the Gaussian width.

In their present form, $\hat{\rho}_c$ and $\hat{\rho}_i$ have an eigenspectrum formed by all combinations of edge and bulk eigenmodes as illustrated in Fig. 2(b). However, to fully exploit topological protection, it is essential that the initial wave packets comprise only edge modes. Otherwise, we would observe decreased performance of the topological system, due to the presence of non-topological bulk modes in the initial states [21,22]. To fulfill this requirement, we project $\hat{\rho}_\alpha$ onto the lattice eigenstates to obtain the spectral representation and set to zero all bulk components; we then renormalize the resulting state and transform it back to the spatial representation. The absolute values of the resulting states are shown in Fig. 2(c). It is important to remark that the bulk-cleaning procedure renders states with a higher

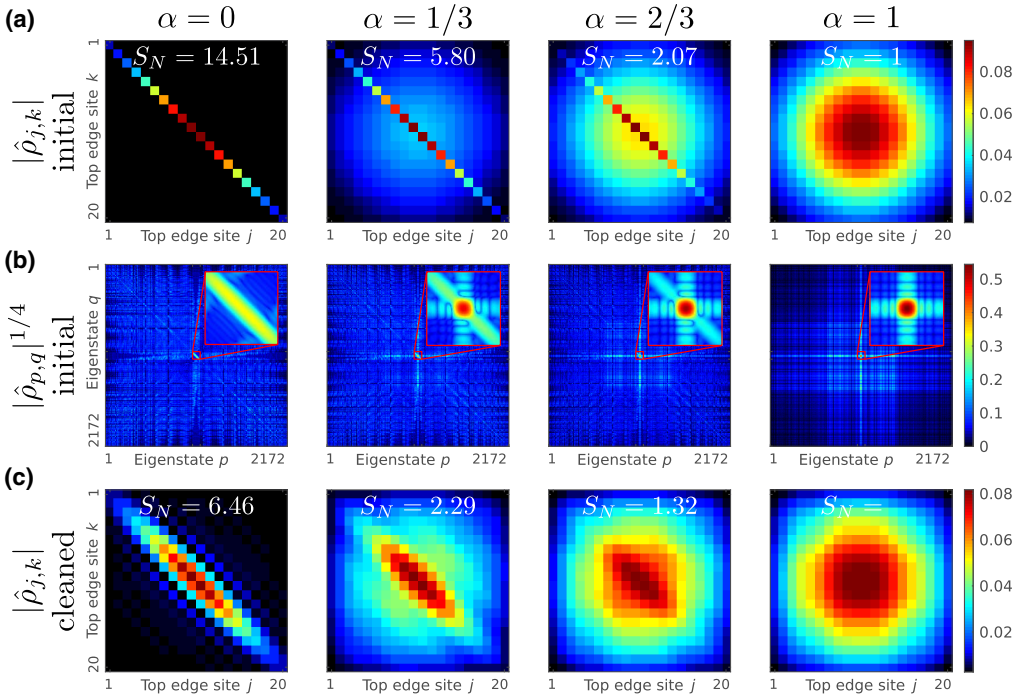

Fig. 2. Initial states. (a) and (b) The absolute values of the spatial $|\hat{\rho}_{j,k}|$ and spectral $|\hat{\rho}_{p,q}|$ coherences, respectively, for some examples of initial states $\hat{\rho}_\alpha$ in the Haldane lattice. To improve the visibility of small components within the spectral edge-edge subspace, the insets in (b) depict $\sqrt[4]{|\hat{\rho}_{p,q}|}$. In (c) we show the spatial coherences $|\hat{\rho}_{j,k}|$ for the states obtained after removing all spectral bulk-bulk components. In all cases, we observe significant changes in the shape of the spatial coherences, and in the most extreme case ($\alpha = 0$), the removal of the spectral bulk components transforms a formerly incoherent state [leftmost panel in (a)] into a partially coherent one [leftmost panel in (c)].

degree of coherence than their incoherent "progenitors," yet the resulting states are never fully coherent. Further, the bulk-cleaning procedure leaves the spatial shape of fully coherent states practically unchanged, while partially coherent and fully incoherent states acquire significantly different spatial shapes, e.g., $\hat{\rho}_i$, which was fully diagonal but now contains some coherences (off-diagonal elements) as shown in the leftmost panel of Fig. 2(c). The emergence of these coherences is our first important result; it clearly implies that to create wave packets comprising only edge modes, it is required to meet a certain degree of spatial coherence. In what follows we use the bulk-free states as initial states.

In a fully coherent scenario, topological protection of the state $\hat{\rho}_c$ manifests as unidirectional energy transport along the lattice's edges with only 1% of the total energy being scattered into the bulk by disorder as depicted in Fig. 3(a). In contrast, for partially coherent light, the disordered region acts as a barrier within which more and more light gets arrested as the degree of coherence decreases as shown in Fig. 3(b). Note that the state $\hat{\rho}_i(\alpha = 0)$ shown in Fig. 3(b) is not fully incoherent, even though it was generated with the coherence parameter $\alpha = 0$. This is due to the bulk-cleaning procedure, which has reintroduced some spatial coherences as can be seen in the bottom-left panel of Fig. 2(c).

To elucidate the impact of disorder on the topological protection of partially coherent light, we examine two figures of merit, the transmittance and the fidelity. The transmittance is defined as the light intensity transferred through the disordered region $T = \sum_j [\hat{\rho}_\alpha(z_l)]_{j,j}$, where $\hat{\rho}_\alpha$ are the evolved states in the disordered lattices, and the sum runs only over the sites in the region to the right of the disordered area. The fidelity F is computed between the states evolved in the disordered lattice $\hat{\rho}_\alpha(z_l)$ and the reference states $\hat{\rho}_{df}(z_f)$ obtained after propagating the same initial state $\hat{\rho}_\alpha(0)$ through a disorder-free lattice. F is given as $F(\hat{\rho}_\alpha(z_l), \hat{\rho}_{df}(z_f)) = 1 - D(\hat{\rho}_\alpha(z_l), \hat{\rho}_{df}(z_f))$, where $D(\hat{\rho}_\alpha(z_l), \hat{\rho}_{df}(z_f)) = \mathrm{Tr}(|\hat{\rho}_\alpha(z_l) - \hat{\rho}_{df}(z_f)|)/2$ is the trace distance that measures the overlap between the light states $\hat{\rho}_\alpha$ and $\hat{\rho}_{df}$ [29]. To be precise, $D = 0$ if and only if $\hat{\rho}_\alpha = \hat{\rho}_{df}$, and $0 < D \leq 1$ stands for the opposite, $\hat{\rho}_\alpha \neq \hat{\rho}_{df}$. In turn, a fidelity of $F = 1$ attests that $\hat{\rho}_\alpha$ has not undergone any deviation from $\hat{\rho}_{df}$, while $0 \leq F < 1$ measures the degree of dissimilarity between both states. Indeed, $F = 1$ is only obtained when both states traverse the same system. Note that z_f is the propagation distance after which $\hat{\rho}_{df}$ has reached the right side of the disorder-free system, that is, the right blue area in the Haldane lattice shown in Fig. 1(a). In the presence of disorder, the states tend to slow down inside the disorder barrier, such that $\hat{\rho}_\alpha(z_f)$ lags behind $\hat{\rho}_{df}(z_f)$. To compensate for this delay, we let the states evolve a slightly larger propagation distance $z_l \in [z_f, z_f + 10]$, such that $F(\hat{\rho}_\alpha(z_l), \hat{\rho}_{df}(z_f))$ is at a local maximum. Further, we only consider the transmitted part of $\hat{\rho}_\alpha(z_l)$ and $\hat{\rho}_{df}(z_f)$ to compute the trace distance D, i.e., their projection onto the clean region to the right of the disorder barrier.

To provide a first insight into the topological protection of partially coherent light, we consider the evolution of $\hat{\rho}_\alpha$ in systems with a relatively high disorder strength $\Delta = 1$. As shown in Fig. 3(c), the degree of coherence μ^2 for the trial states $\hat{\rho}_\alpha$ is an increasing function of α with an upper bound $\mu^2 = 1$ for the fully coherent case ($\alpha = 1$). For fully coherent states ($\alpha = 1$), the Haldane lattice allows for a fidelity $F \approx 0.9$ [Fig. 3(e)] and a nearly perfect transmittance $T \approx 0.99$ [Fig. 3(d)]. However, as the degree of coherence decreases ($\alpha \to 0$), both figures of merit T and F drop to about 0.6 [Figs. 3(e) and 3(f)]. In other

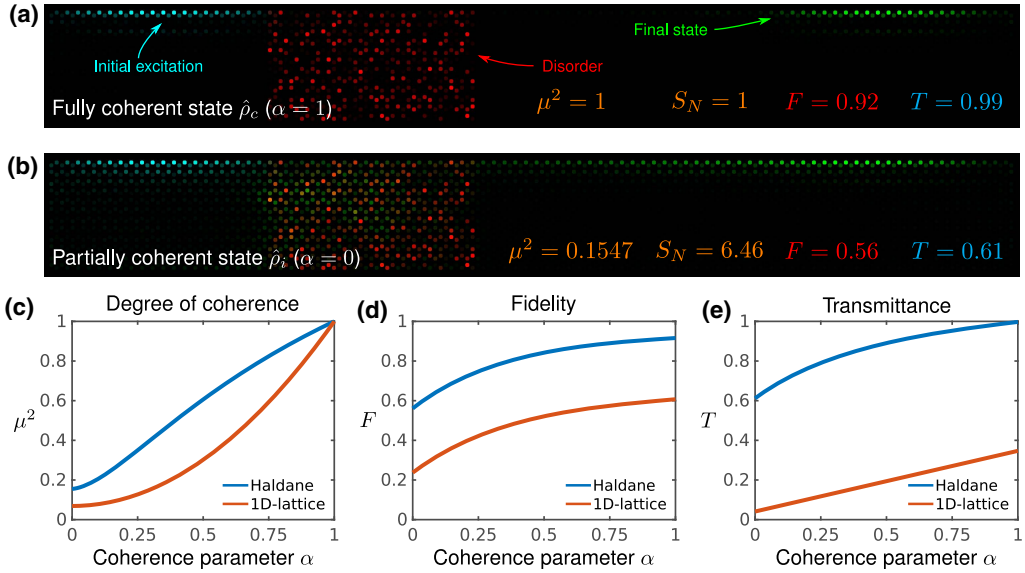

Fig. 3. Topological protection of coherent and partially coherent light states. (a) and (b) The initial and final intensities of the coherent $\hat{\rho}_c$ and the partially coherent $\hat{\rho}_i$ states, respectively. Both states are initialized with a Gaussian width $\sigma = 6$, and the lattices exhibit a disorder strength $\Delta = 1$. After a propagation distance of $z = 75$, both states reach the right side of the lattice. While the fully coherent excitation (a) freely passes through the disorder barrier, (b) the partially coherent state scatters into the bulk. Note that the cyan (green) spots indicate the intensity distribution of the initial (final) state, while the red spots show the disorder distribution. In (c)–(e) we show the degree of coherence μ^2, fidelities, and transmittances as a function of the coherence parameter α for the states $\hat{\rho}_\alpha$ in systems with disorder strength $\Delta = 1$.

words, even for the most incoherent states analyzed here, up to 60% of the total energy is topologically protected because it gets through the disordered barrier, while 40% is scattered into the bulk.

To spotlight the advantages provided by topological protection, we have performed the corresponding analysis for a one-dimensional disordered lattice and the topologically trivial Haldane lattice. Here, we present the results for the 1D lattice, while the results for the trivial Haldane model are given in Appendix A. The coupling matrix elements for this 1D system are given by $H_{m,n} = \kappa(\delta_{m+1,n} + \delta_{m-1,n}) + \delta_{m,n}\Delta_n$, where κ represents the coupling coefficients between nearest-neighbor waveguides, and Δ_n represents the random on-site refractive index implemented in the same way as for the Haldane lattice [Fig. 1(b)]. In the absence of disorder, the spectrum of a 1D lattice comprising M waveguides is analytically given as $\lambda_n = -2\kappa \cos(\pi n/(M+1))$, which in Liouville space acquires the form $\Lambda_{p,q} = -2\kappa \cos(\pi p/(M+1)) + 2\kappa \cos(\pi q/(M+1))$ [Fig. 1(b)]. Notice that in this case the initial excitations are constructed in the same way as for the Haldane lattice, with the obvious exception of the bulk-cleaning procedure. Computation of the transmittance and fidelity reveals that, in 1D lattices, even fully coherent states cannot withstand the impact of disorder at the same level as the worst partially coherent case in the Haldane lattice: the best transmittance and fidelity for the 1D lattice are found to be $T \approx 0.38$ and $F \approx 0.6$ for fully coherent states; see Figs. 3(d) and 3(e).

We now examine the parameter regime within which partially coherent light experiences topological protection. To do so, we compute the transmittances for states $\hat{\rho}_\alpha$ with degree of coherence $\alpha \in [0,1]$, traversing lattices with disorder strengths $\Delta \in [0,2]$. The results are summarized in Fig. 4. As clearly seen in Fig. 4(a), irrespective of the coherence parameter α, partially coherent states endure much stronger disorder [see the red area bounded by the contour line 0.9 in Fig. 4(a)], and they allow transmittances $T > 0.9$ for disorder strengths as high as $\Delta = 1.4$. Even more intriguingly, our estimates reveal that the most incoherent cases ($\alpha = 0$) exhibit transmittances $T > 0.8$ for disorder strengths $\Delta \in [0,0.5]$. That is, even when the disorder closes the bandgap from (−1,1), as indicated by the blue region in the spectrum of Fig. 1(a), to (−0.8,0.8) for $\Delta = 0.5$, the most incoherent states show a considerable robustness to the impact of disorder.

To grasp these results we refer to the eigenspectra shown in the insets of Fig. 2(b) and notice that in the topological lattice, as the states become more incoherent, they tend to populate edge-edge coherences that are spectrally close to the bulk-bulk and edge-bulk subspaces. As a result, any perturbation or disorder unavoidably induces substantial overlap of edge-edge and bulk-bulk coherences, leading to localization of light into the disorder barrier and thereby preventing energy transport through it.

Correspondingly, for a disorder-free 1D lattice ($\Delta = 0$), we find that a minimum value of $\alpha \approx 0.8$ is required to obtain a transmittance of $T = 0.9$, and $T > 0.9$ can only be obtained for fully coherent states ($\alpha = 1$) and weak disorder ($\Delta < 0.5$). However, by gradually increasing the disorder strength, the transmittance quickly drops to 0 [Fig. 4(b)]. This poor performance in the transport of energy occurs because for $\alpha < 1$ the light states suffer from backscattering more prominently than the highly coherent ones ($\alpha = 1$). Clearly, the clean and disordered cases behave entirely differently; as a result of backscattering, partially coherent fields are destroyed in non-topological lattices, while in topological lattices partially coherent light still experiences a high degree of protection as described above.

In the presence of disorder, the spectral bandgap of a photonic topological insulator becomes narrower, and this process allows the coupling between intermediate energy bulk states and the edge modes with the lowest and largest energy within the bandgap. Such a coupling unavoidably increases as the spatial extension of the initial states becomes smaller. To quantify the effects of the corresponding disorder-induced coupling for partially coherent light, we consider light states exhibiting

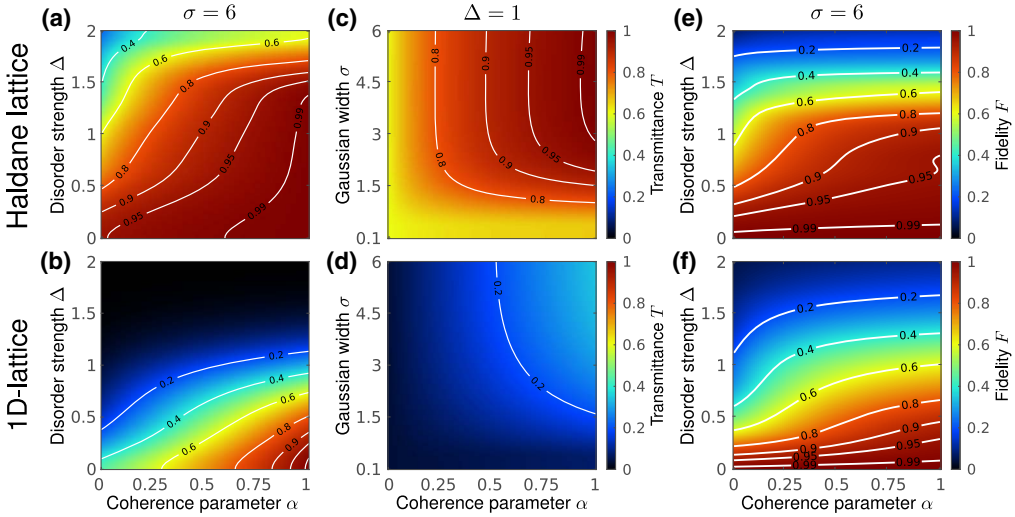

Fig. 4. Transmittance and fidelity versus disorder strength Δ, spatial width σ, and degree of coherence of the initial states. (a) and (b) The transmittance T for the Haldane lattice and the 1D lattice versus the disorder strength $\Delta \in [0,2.5]$ and α, for initial states with a Gaussian width $\sigma = 6$. Similarly, (c) and (d) show T as a function of α for initial excitations with spatial widths $\sigma \in [0.1,6]$ in lattices with disorder strength $\Delta = 1$. (e) and (f) The fidelity F as a function of Δ and α for light states with spatial width $\sigma = 6$.

spatial widths in the range $\sigma \in [0.1,6]$ propagating in systems with relatively high disorder strength $\Delta = 1$. We find that states with widths $\sigma \in [1.5,6]$ and coherence parameters $\alpha \in [0.25,1]$ achieve transmittances $T > 0.8$ [Fig. 4(c)]. Hence, we can define the threshold ($\alpha = 0.25, \sigma = 1.5$) above which partially coherent light presents the highest transmittances. For the 1D lattice, the width of the states plays no role, and the transmittance remains below 0.4 in the whole range $\alpha \in [0,1]$ and $\sigma \in [0,6]$ [Fig. 4(d)].

We now study the fidelity as a function of the coherence parameter $\alpha \in [0,1]$ and the disorder strength $\Delta \in [0,2]$ for states $\hat{\rho}_\alpha$ with a fixed width $\sigma = 6$. In agreement with the transmittance analysis, all the initial states render the same threshold $F \geq 0.8$ in the whole coherence interval $\alpha \in [0,1]$ for the same levels of disorder $\Delta \in [0,1]$ [Fig. 4(e)]. For the trivial 1D case, $F \geq 0.8$ is encountered for very weak disorder $\Delta \leq 0.5$, and the equality $\Delta = 0.5$ only holds for fully coherent states; see Fig. 4(f). This clearly shows that the fidelity response of the 1D lattice is always outperformed by the photonic topological insulator. The analysis for the topologically trivial Haldane system, which yields a worse transmittance and fidelity response than the 1D lattice, leads to the same conclusions; see Appendix A.

3. PROTECTION WINDOW

We have found that partially coherent light can be structured to possess relatively high topological immunity. Concomitantly with the drop in the degree of coherence, the corresponding eigenspectra extend over the bulk-bulk and edge-bulk subspaces, causing rapid deterioration of the wave packets after propagating through disorder. Hence, the key to optimize topological protection for partially coherent light is to minimize the coupling induced by disorder of the initial spectrum with the edge-bulk and bulk-bulk spectral regions. This optimization can be achieved by first noting that for every instance of disorder Δ, there exists a different spectral window within which light states enjoy topological protection. To deduce the protection window, we launch a spatially very narrow fully coherent bulk-cleaned excitation through an ensemble of $N = 5000$ disordered Haldane lattices. In Figs. 5(a)–5(c), we show the ensemble average of the spectral coherences after propagation through disorder $\langle |\hat{\rho}_{p,q}(z_f)| \rangle_N$. In the disorder-free case ($\Delta = 0$), we observe that the spectral coherences remain invariant; $\langle |\hat{\rho}_{p,q}(z_f)| \rangle_N = |\hat{\rho}_{p,q}(0)|$. One can see that the only surviving spectral intensities and coherences lie in a square region, the spectral window of topological protection, which shrinks with increasing levels of disorder. From these results it easy to see why even the bulk-cleaned states are not completely protected by topology. As shown in the insets of Fig. 2(b), when the coherence parameter α is below 1, the spectral coherences acquire an elongated elliptical shape in the edge-edge subspace. Depending on the strength of the disorder, the tails of the ellipse may fall outside of the window of protection, facilitating the scattering into the bulk, resulting in reduced transmittance and fidelity.

Before concluding, it is worth to briefly comment on the stages to demonstrate topological protection of partially coherent light experimentally. First, partially coherent light states $\hat{\rho}(\alpha)$ can be readily produced using a spatial light modulator [30], to stochastically generate the coherent modes in $\hat{\rho}(\boldsymbol{x}_1, \boldsymbol{x}_2) = \sum_k \lambda_k \varphi_k^*(\boldsymbol{x}_1)\varphi_k(\boldsymbol{x}_2)$ [31]. The Haldane lattice and other topological lattice systems can be implemented using femtosecond laser writing techniques in fused silica as demonstrated in Ref. [4]. The on-site disorder can be implemented by varying the writing velocity of the waveguides to modify the propagation constants [32]. Alternatively, one-dimensional topological lattices, such as the Su–Schrieffer–Heeger (SSH) lattice, can be implemented using silicon nanowires as shown in Refs. [20,33]. As we show in Appendix A, topological effects also endure under partial coherence in SSH lattices. Thus, these types of experiments can be realistically carried out.

4. CONCLUSION

We have demonstrated that partially coherent light survives randomness associated with disordered photonic topological insulators. This is in stark contrast with the case of non-topological systems, where light excitations deteriorate very quickly when full coherence cannot be achieved. We have shown that the vulnerability of the partially coherent states is due to the inherent overlap of the spectrum with the bulk-bulk and bulk-edge coherences. Hence, to grant topological protection to partially coherent light, we have to keep the spectral coherence maps in the center of a well-defined spectral window: the topological window of protection. This condition of course limits the degree of spatial coherence that guarantees robustness

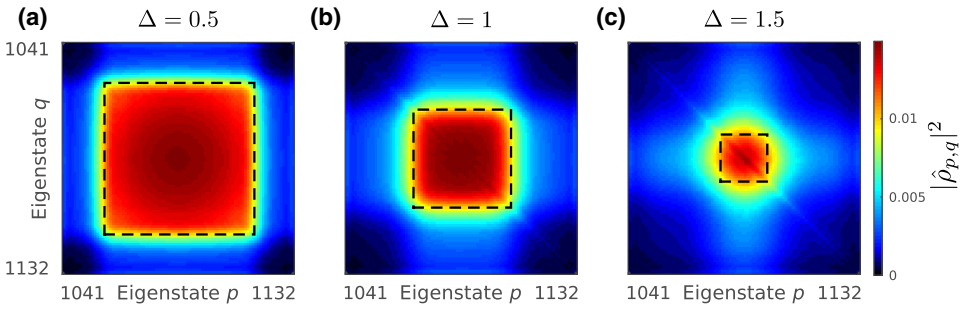

Fig. 5. The topological window of protection. To identify the topological window of protection, we considered a spectrally broad (spatially narrow) partially coherent state with $\sigma = 0.1$ as the initial state and propagate it through an ensemble of 5000 random Haldane lattices. In disorder-free systems, the spectral correlation map remains intact. As the disorder strength increases, e.g., (a) $\Delta = 0.5$, (b) $\Delta = 1$, and (c) $\Delta = 1.5$, the bandgap reduces, yielding to a reduction of the spectral window of protection as indicated by the dashed squares shown in the edge-edge subspace.

of light. Yet, it presents an important tool to define the precise coherence attributes of light in order to be protected in topological insulators. This is especially important, since, in a real-world scenario, perfectly coherent light is unobtainable. Thus, our work is of considerable interest for the development of, for example, topological optical computing and information processing systems [34,35]. As we have shown, the full-coherence condition for the initial light fields can be relaxed, and the advantages offered by topology can be enjoyed using only partially coherent beams. This opens up the design space to a wider selection of light sources, possibly yielding smaller, cheaper, and more robust devices based on the topological transport of light.

APPENDIX A

1. Topologically Trivial Haldane Lattice

We analyze the transmittance and fidelity of partially coherent light states in the disordered, topologically trivial Haldane lattice. To achieve the trivial phase, we choose the Haldane flux $\varphi = 0$. To maintain the comparability with the results from the main text, we set the nearest-neighbor coupling $\kappa_1 = 1$ and the next-nearest-neighbor coupling $\kappa_2 = 0.2$. Since the system exhibits no topological edge modes, we have to adapt our choice for the initial states. Thus, we start with the 2D-Gaussian wave packet

$$E_m = A e^{-ik_x x_m} e^{-ik_y y_m} e^{-\frac{(x_m - x_0)^2}{2\sigma_x^2}} e^{-\frac{(y_m - y_0)^2}{2\sigma_y^2}}, \tag{A1}$$

centered at $(x_0, y_0) \approx (10.5, 5.5)$ (in units of the next-nearest-neighbor distance), with spatial widths $\sigma_x = 6, \sigma_y = 1.5$ and momentum $k_x = \pi/\sqrt{2}, k_y = 0$ as indicated by the cyan dots in Fig. 6(a). After the propagation distance $z_f = 40$ in the clean lattice, the completely coherent wave packet $\hat{\rho}_c = \boldsymbol{E} \otimes \boldsymbol{E}^\dagger$ has indeed reached the right-hand-side of the lattice; see the green dots in Fig. 6(a). We now launch the completely coherent state through a moderate amount of disorder $\Delta = 0.5$, and we see that a significant amount of the intensity is either backscattered or stuck in the disordered region in Fig. 6(b). This is the first indication that the trivial Haldane phase will perform significantly worse than the topological one. To further investigate, we measure the transmittance T and fidelity F (as was done in the main text) against the disorder strength Δ and the coherence parameter α. The results are shown in Figs. 6(c) and 6(d). As expected, the trivial phase is outperformed by the topological phase in the complete parameter regime (Δ, α). Remarkably, the trivial Haldane lattice is likewise outperformed by the trivial 1D lattice. For fully or mostly coherent light, the reason is that 2D forward scattering occurs only within a relatively small range of angles. However, in a 1D setting, there exists only forward and backward scattering, which significantly enhances forward scattering and thereby improves the transmittance and fidelity with respect to the 2D case. Furthermore, completely incoherent light states lose all their momentum in the topologically trivial systems. However, this is partially compensated for in the 1D case, where a significant amount of diffraction occurs along propagation. This enables some of the intensity to leak beyond the disorder barrier in the 1D lattice. But, in the 2D case, the diffraction in x direction is too slow to yield a similar effect, leading to a further decrease in the transmittance for partially coherent and fully incoherent light.

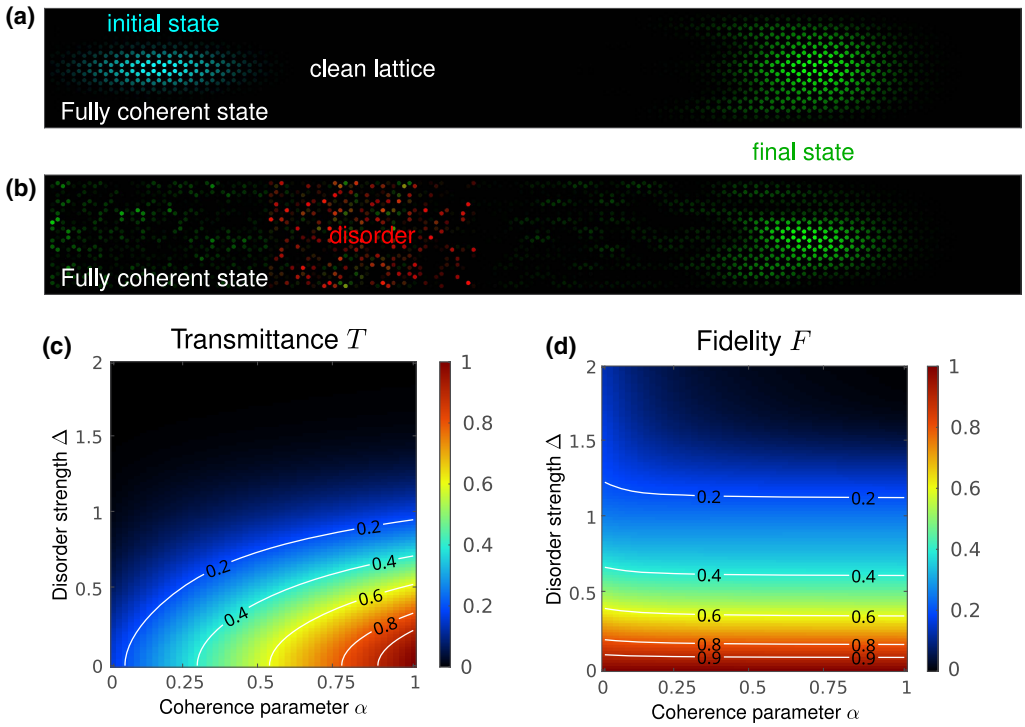

Fig. 6. Trivial Haldane lattice. Fully coherent state evolution in (a) the clean and (b) the disordered system. (c) Transmittance and (d) fidelity scans over disorder strength and coherence parameter.

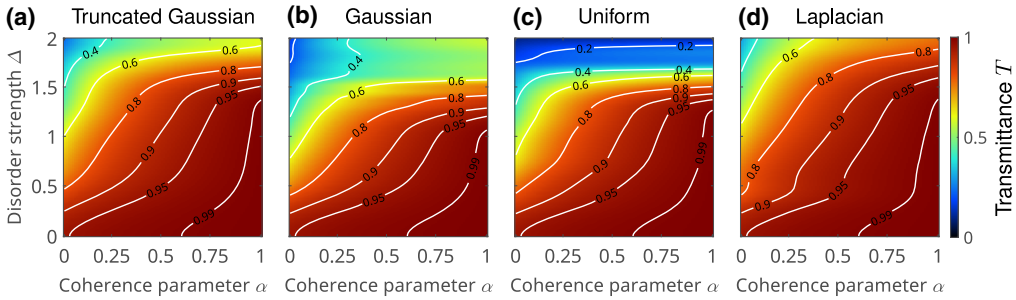

Fig. 7. Transmittance versus disorder strength and coherence parameter in the topological Haldane lattice for different disorder distributions. (a) Truncated Gaussian. (b) Gaussian. (c) Uniform. (d) Laplacian.

2. Random Disorder Distributions

We now investigate the impact of different disorder distributions on our results. To this end, we perform again the parameter scans of the transmittance over (Δ, α) (topological non-trivial Haldane lattice) for three other probability distributions. Explicitly, we choose a non-truncated Gaussian, a uniform, and a Laplace distributions. To reiterate, in the main text we have implemented the random on-site disorder in the refractive indices β_j via a truncated Gaussian distribution. To be precise, before the truncation, we choose the Gaussian variance as $\sigma^2 = 1$. The truncation to the interval $[-\sqrt{2}, \sqrt{2}]$ renders a final distribution with an effective variance of $\sigma_{\text{eff}}^2 = 0.5$. After drawing the ensemble of random numbers r_j, they are then multiplied by the disorder strength to obtain the refractive indices $\beta_j = r_j\Delta$. Thus, to obtain comparable results, we have ensured that the variance of the new distributions of the r_j is equal to 0.5. As one can see in Fig. 7, we indeed obtain very similar results in all four cases. Our results are therefore not significantly sensitive to the specific disorder distribution at hand.

3. Partially Coherent Stationary Modes

We consider the effects of partial coherence on edge modes in the SSH model. The SSH model is particularly convenient for experimental realization [20,33], since it requires only a 1D lattice of waveguides with alternating strong (κ_1) and weak (κ_2) coupling coefficients between nearest neighbors. To obtain a similar bandgap as in the Haldane lattice, we choose $\kappa_1 = 1$ and $\kappa_2 = 0.2$. Specifically, we consider an SSH chain of $M = 101$ waveguides, exhibiting a defect at the center waveguide as shown in Fig. 8(a). This defect gives rise to a zero-energy topological mode, which is strongly localized around the center waveguide (and the odd-numbered waveguides around it). Evidently, such a topological mode exhibits no momentum, and therefore it is impossible to "send" through a region of static disorder. Thus, due to the stationary nature of the SSH defect mode, a scattering-based transmittance analysis, as was done in the main text, is unfeasible.

Instead, we will apply static disorder across the complete lattice and then let the initial light state evolve for a fixed propagation distance $z_f = 20$. We then calculate the "bound intensity" $I_b(z) = \sum_n \hat{\rho}_{n,n}(z)$ in the waveguides $n \in [n_c - 5, n_c + 5]$. Since the initial topological mode exhibits $I_b(0) = 0.99994 \approx 1$, this quantity will indicate how much of the total intensity remains bound to the region of the defect mode after the evolution in the disordered system. In other words, I_b indicates the amount of light that has resisted the leakage into the bulk due to disorder. As the second observable, we use the fidelity F as we have defined in the main text. For comparison, we measure the same observables in a regular lattice exhibiting a non-topological defect mode as shown in Fig. 8(b).

In Figs. 8(c)–8(f), we show the results of the parameter scans of I_b and F over the disorder strength and coherence parameter. Quite remarkably, the bound intensity I_b remains above 0.9 in the complete parameter range for the SSH model.

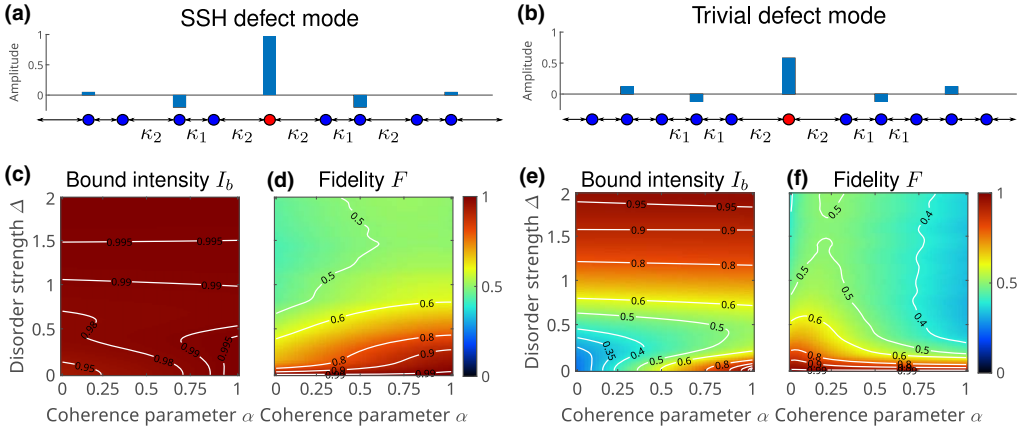

Fig. 8. Stationary defect modes in 1D arrays. (a) Topological defect mode of an SSH lattice. (b) Trivial defect mode of a regular lattice. (c), (d) Bound intensity and fidelity against disorder strength and coherence parameter in the SSH system and (e), (f) in the regular lattice.

This indicates that even a completely incoherent excitation of the defect mode will remain tightly bound despite extreme disorder. Note that the minimum value for $I_b \approx 0.94$ is reached for $\Delta = 0 = \alpha$, that is, in the absence of disorder and coherence. Counterintuitively, keeping $\alpha = 0$ and increasing the level of disorder causes I_b to increase as well. This seems to indicate that the disorder causes an Anderson localization effect [36], which counteracts the diffraction due to the lack of coherence in the initial excitation. Since the trivial defect mode exhibits $I_b(0) \approx 0.38$, we show the normalized bound intensity $I_b/I_b(0)$ in Fig. 8(e). In principle, this "favors" the trivial defect mode, but in spite of this we still observe a significant advantage for the topological system. We observe the same with regards to the fidelity response, where the SSH lattice also outperforms the trivial 1D lattice.

Acknowledgements. K.T., A.P.L., and K.B. acknowledge support by the Deutsche Forschungsgemeinschaft (DFG) within the framework of the DFG priority program 1839 Tailored Disorder (BU 1107/12-2, PE 2602/2-2).

Disclosures. The authors declare that there are no conflicts of interest related to this article.

Data Availability. Data underlying the results presented in this paper are not publicly available at this time but may be obtained from the authors upon reasonable request.

REFERENCES

1. Z. Wang, Y. Chong, J. D. Joannopoulos, and M. Soljačić, "Observation of unidirectional backscattering-immune topological electromagnetic states," Nature **461**, 772–775 (2009).
2. F. D. M. Haldane, "Model for a quantum Hall effect without landau levels: condensed-matter realization of the 'parity anomaly'," Phys. Rev. Lett. **61**, 2015–2018 (1988).
3. C. He, H.-S. Lai, B. He, S.-Y. Yu, X. Xu, M.-H. Lu, and Y.-F. Chen, "Acoustic analogues of three-dimensional topological insulators," Nat. Commun. **11**, 2318 (2020).
4. M. C. Rechtsman, J. M. Zeuner, Y. Plotnik, Y. Lumer, D. Podolsky, F. Dreisow, S. Nolte, M. Segev, and A. Szameit, "Photonic Floquet topological insulators," Nature **496**, 196–200 (2013).
5. A. B. Khanikaev, S. Hossein Mousavi, W.-K. Tse, M. Kargarian, A. H. MacDonald, and G. Shvets, "Photonic topological insulators," Nat. Mater. **12**, 233–239 (2013).
6. M. Hafezi, S. Mittal, J. Fan, A. Migdall, and J. M. Taylor, "Imaging topological edge states in silicon photonics," Nat. Photonics **7**, 1001–1005 (2013).
7. K. Fang, Z. Yu, and S. Fan, "Realizing effective magnetic field for photons by controlling the phase of dynamic modulation," Nat. Photonics **6**, 782–787 (2012).
8. M. Hafezi, E. A. Demler, M. D. Lukin, and J. M. Taylor, "Robust optical delay lines with topological protection," Nat. Phys. **7**, 907–912 (2011).
9. Y. Poo, R.-X. Wu, Z. Lin, Y. Yang, and C. T. Chan, "Experimental realization of self-guiding unidirectional electromagnetic edge states," Phys. Rev. Lett. **106**, 093903 (2011).
10. X. Zhang, M. Xiao, Y. Cheng, M.-H. Lu, and J. Christensen, "Topological sound," Commun. Phys. **1**, 97 (2018).
11. Z. Yang, F. Gao, X. Shi, X. Lin, Z. Gao, Y. Chong, and B. Zhang, "Topological acoustics," Phys. Rev. Lett. **114**, 114301 (2015).
12. L. Lu, J. D. Joannopoulos, and M. Soljačić, "Topological photonics," Nat. Photonics **8**, 821–829 (2014).
13. M. A. Bandres, S. Wittek, G. Harari, M. Parto, J. Ren, M. Segev, D. N. Christodoulides, and M. Khajavikhan, "Topological insulator laser: experiments," Science **359**, eaar4005 (2018).
14. G. Harari, M. A. Bandres, Y. Lumer, M. C. Rechtsman, Y. D. Chong, M. Khajavikhan, D. N. Christodoulides, and M. Segev, "Topological insulator laser: theory," Science **359**, eaar4003 (2018).
15. M. A. Bandres, M. C. Rechtsman, and M. Segev, "Topological photonic quasicrystals: fractal topological spectrum and protected transport," Phys. Rev. X **6**, 011016 (2016).
16. S. Stützer, Y. Plotnik, Y. Lumer, P. Titum, N. H. Lindner, M. Segev, M. C. Rechtsman, and A. Szameit, "Photonic topological Anderson insulators," Nature **560**, 461–465 (2018).
17. Z. Yang, E. Lustig, Y. Lumer, and M. Segev, "Photonic Floquet topological insulators in a fractal lattice," Light Sci. Appl. **9**, 128 (2020).
18. M. C. Rechtsman, Y. Lumer, Y. Plotnik, A. Perez-Leija, A. Szameit, and M. Segev, "Topological protection of photonic path entanglement," Optica **3**, 925–930 (2016).
19. S. Mittal, V. V. Orre, and M. Hafezi, "Topologically robust transport of entangled photons in a 2D photonic system," Opt. Express **24**, 15631–15641 (2016).
20. A. Blanco-Redondo, B. Bell, D. Oren, B. J. Eggleton, and M. Segev, "Topological protection of biphoton states," Science **362**, 568–571 (2018).
21. K. Tschernig, Á. Jimenez-Galán, D. N. Christodoulides, M. Ivanov, K. Busch, M. A. Bandres, and A. Perez-Leija, "Topological protection versus degree of entanglement of two-photon light in photonic topological insulators," Nat. Commun. **12**, 1974 (2021).
22. K. Tschernig, R. L. Franco, M. Ivanov, M. A. Bandres, K. Busch, and A. Perez-Leija, "Topological protection of highly entangled non-Gaussian two-photon states," Mater. Quantum Technol. **1**, 035001 (2021).
23. C. Doyle, W.-W. Zhang, M. Wang, B. A. Bell, S. D. Bartlett, and A. Blanco-Redondo, "Biphoton entanglement of topologically distinct modes," Phys. Rev. A **105**, 023513 (2022).
24. Y. Deng and D. Chu, "Coherence properties of different light sources and their effect on the image sharpness and speckle of holographic displays," Sci. Rep. **7**, 5893 (2017).
25. A. Eckardt and E. Anisimovas, "High-frequency approximation for periodically driven quantum systems from a Floquet-space perspective," New J. Phys. **17**, 093039 (2015).
26. E. Wolf, *Introduction to the Theory of Coherence and Polarization of Light* (Cambridge University, 2007).
27. M. Alonso, T. Setälä, and A. T. Friberg, "Minimum uncertainty solutions for partially coherent fields and quantum mixed states," New J. Phys. **16**, 123023 (2014).
28. J. Sperling and W. Vogel, "The schmidt number as a universal entanglement measure," Phys. Scripta **83**, 045002 (2011).
29. A. Smirne, S. Cialdi, G. Anelli, M. G. A. Paris, and B. Vacchini, "Quantum probes to experimentally assess correlations in a composite system," Phys. Rev. A **88**, 012108 (2013).
30. V. Arrizon, U. Ruiz, R. Carrada, and L. A. Gonzalez, "Pixelated phase computer holograms for the accurate encoding of scalar complex fields," J. Opt. Soc. Am. A **24**, 3500–3507 (2007).
31. Y. Lumer, Y. Liang, R. Schley, I. Kaminer, E. Greenfield, D. Song, X. Zhang, J. Xu, Z. Chen, and M. Segev, "Incoherent self-accelerating beams," Optica **2**, 886–892 (2015).
32. R. Keil, A. Perez-Leija, P. Aleahmad, H. Moya-Cessa, S. Nolte, D. N. Christodoulides, and A. Szameit, "Observation of Bloch-like revivals in semi-infinite Glauber–Fock photonic lattices," Opt. Lett. **37**, 3801–3803 (2012).
33. A. Blanco-Redondo, I. Andonegui, M. J. Collins, G. Harari, Y. Lumer, M. C. Rechtsman, B. J. Eggleton, and M. Segev, "Topological optical waveguiding in silicon and the transition between topological and trivial defect states," Phys. Rev. Lett. **116**, 163901 (2016).
34. M. Makwana, R. Craster, and S. Guenneau, "Topological beam-splitting in photonic crystals," Opt. Express **27**, 16088–16102 (2019).
35. Y.-F. Gao, J.-P. Sun, N. Xu, Z. Jiang, Q.-C. Hou, H. Song, M.-C. Jin, and C. Zhang, "Manipulation of topological beam splitter based on honeycomb photonic crystals," Opt. Commun. **483**, 126646 (2021).
36. L. Martin, G. D. Giuseppe, A. Perez-Leija, R. Keil, F. Dreisow, M. Heinrich, S. Nolte, A. Szameit, A. F. Abouraddy, D. N. Christodoulides, and B. E. A. Saleh, "Anderson localization in optical waveguide arrays with off-diagonal coupling disorder," Opt. Express **19**, 13636–13646 (2011).